ISSN 8755-6839

SCIENCE OF TSUNAMI HAZARDS

Journal of Tsunami Society International

Volume 34 Number 4 2015

COMPARATIVE NUMERICAL SIMULATION OF THE TOHOKU 2011 TSUNAMI

Baranova N.A.[1], Kurkin A.A.[1], Mazova R.Kh.[1], Pararas-Carayannis, G.[2]

[1]R.E.Alekseev Nizhny Novgorod State Technical University, Nizhny Novgorod, Russia
[2]Tsunami Society International, Honolulu, Hawaii, USA

ABSTRACT

The comparative numerical simulation of generation and propagation of tsunami waves generated by the source of the catastrophic 2011 Tohoku earthquake in Japan was performed based on the Okada model and the dynamic keyboard block model. The initial model is connected with the choice of orientation of longitudinal and transverse ruptures within the source region and the values of displacements along the main fault. A subsequent model is based on the premise that the initial stress distribution along the fault zone affects essentially the character of movements around the earthquake source and takes into account the stress-strain state of keyboard blocks. In the first case of the present study, the earthquake source was designated and constructed based on the parameters of the ten largest aftershocks within a finite time interval, while in the second case the source used included all aftershocks on the first day following the main event. Based on such comparative source simulations and far-field tsunami wave measurements, the results with both models were determined to have close similarities. However, in the near-field zone, the agreement with observable data was not as good. That can be attributed to inaccuracies in the placement of virtual tide gauges relative to real ones, as well as to features of bottom relief near the coast.

Keywords: *earthquake and tsunami of 2011 Tohoku, earthquake sources, tsunami source, tsunami modeling.*

Vol. 34, No. 4, page 212 (2015)

1. INTRODUCTION

On 11 March 2011, a great earthquake with Moment Magnitude of Mw = 9 occurred along the northeast offshore area of Honshu Island, in Japan. As noted in the scientific literature, this earthquake was much stronger than what had been expected. The sudden shift of the sea floor and the overall displacements generated tremendous tsunami waves, which, within minutes, struck the coasts of Honshu and Hokkaido Islands. The catastrophic waves ranged from 3 to 15 meters in height, destroyed many coastal cities and villages, killed more than 28,000 people and left about 500,000 more homeless. In certain areas and coastal valleys the waves inundated to a distance of up to 10 km inland (see, e.g. (10, 11, 21, 22, Lay and Kanamori 2011), causing colossal material damage. The waves destroyed the water-cooling units of the Fukushima-Daichi nuclear power plant, which led to a catastrophic eruption of radiation (10,11,21, Saito et al. 2011; Pararas-Carayannis 2014). There were power outages for about 4 million homes in Tokyo and the surrounding areas. The disaster left about 4.4 million homes in northeastern Japan without electricity and 1.4 million without water. Early estimates indicated that the monetary losses would far exceed $100 billion (Pararas-Carayannis 2014).

Comparing the Tohoku 11 March 2011 earthquake with predecessor events near the Sanriku coast, it can be determined that it was a typical example of a complex event including in all features of different types of catastrophic earthquakes (Fujii 2011). The process of propagation of the rupture in the source of this event occurred with a cascading failure mechanism, which was difficult to predict, and such a scenario of earthquake was not anticipated in any model of estimating seismic danger (Fujii 2011). A review of the combined rupturing impact on both the subducting Pacific oceanic lithosphere and on the overriding Eurasian tectonic plate (Pararas-Carayannis 2014), confirmed large vertical and horizontal tectonic crustal displacements by the quake's slow and long rupturing process, the three-dimensional dynamics of shallow and deeper subduction processes - as indicated by a spatial and a time sequence distribution and clustering of aftershocks - as well as effects of co-seismic lateral movements which compressed and deformed the sediments along the accretionary prism of the overriding plane near the Japan Trench.

1.1 Earthquake source of the Tohoku 11 March 2011 event.

The epicenter of main shock was located at 38.10° N, 142.86° E. The quake had a focal depth H=24 km, and a moment magnitude M_w=9.0 (21). It occurred about 373 kilometers (231 miles) away from Tokyo, about 130 kms (81 mi) off the east coast of Oshika Peninsula and about 150 km west of the tectonic boundary of the Eurasian and Pacific plates, characterized by the Japan Trench. Strong ground motions were felt as far away as Tokyo (Pararas-Carayannis 2014).

The extent of the source of aftershock distribution during the first day had dimensions of about 300x500 km, covering an area nearly 150,000 km². As described in a number of investigations (see, e.g. (11, Fujii 2011, Koper et al. 2011, Kanamori, 2011, Pararas-Carayannis 2014), the rupture begun very slow at the depth in 23-24 km. Within 45 sec after the onset of the earthquake there was sudden destruction of the accretionary wedge on the upper edge near the plate boundary along the Japan Trench. The affected area had dimensions of about 250×80 km^2

and produced displacements of up to 60 m. The rupture on the wedge along the trench continued for over 135 seconds and terminated near 36.5° S and near 39.5° N (10,11,21,22, Saito et. al. 2011, Fujii 2011). Further examination of the aftershock distribution (Pararas-Carayannis 2014) indicated three major clusters and that the seismic energy of the 2011 earthquake was mainly released about 100 km off the coast of Miyagi and Fukushima Prefectures. Plotting the aftershock focal depths along eastern Honshu by the same study, indicated that there was a spectacular peak of aftershocks at a focal depth of about 24 km, the depth at which the rupture begun. The significance of this to tsunami generation was evaluated in terms of regional, spatial subduction, geometry, slip, crustal movements and sediment displacements. Buckling of the crust due to subduction friction probably activated many minor, normal faults, which also gave rise to subsequent aftershocks - even outside the tsunami generating region on the outer ridge of the subducting plate. Indeed the aftershock distribution was extensive, confirming that the tsunami source area was indeed about 300 km wide and 500 km long (Pararas-Carayannis 2014).

A number of other investigations (Fujii 2011, Koper et al. 2011, Hirose 2011, Ito et al. 2011) also confirmed considerable displacements within the source region. The eastern coast of Japan moved eastward for up to 5 meters and subsided nearly to 1 meter, while the sea floor uplifted on the average of 5 m over an area of about 15,000 km2 (fig.1).

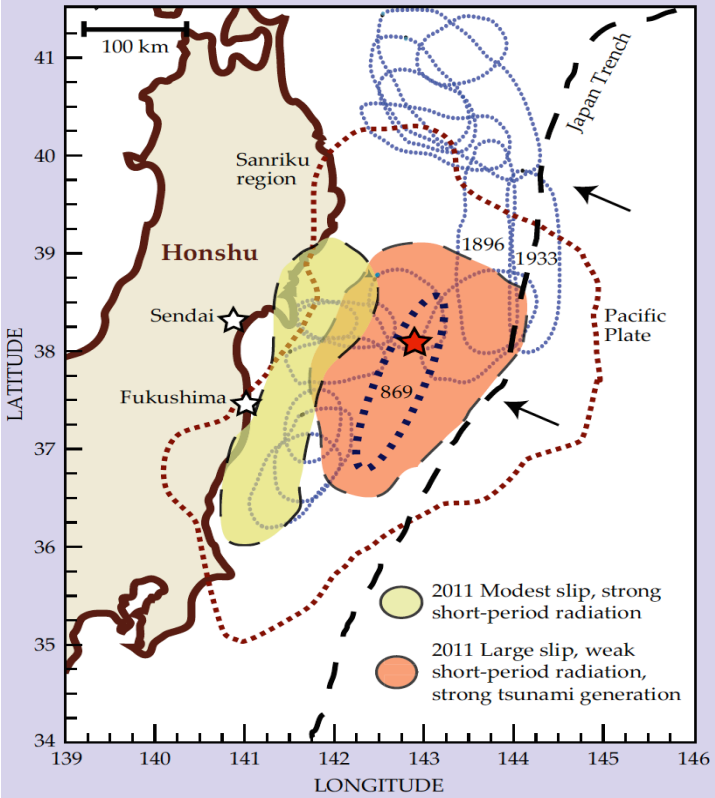

Figure 1. Seismic source of earthquake in Tohoku 11 March 2011 (Fujii 2011).

The direct measurements of sea bottom deformations had a maximum of 60-80 m along the outer portion of the accretionary ridge near the trench. Fig. 1 shows the approximate dimensions of the earthquake source (Fujii 2011) and the red asterisk the epicenter of the main shock of the 2011

earthquake and outlines the approximate area of subduction under the Island of Honshu (Hirose 2011). The black arrows indicate the direction of the Pacific plate motion relative to the Japanese volcanic arc. The area with the light-green color corresponds to the region of gradual shifts and the area with the dark-red color corresponds to the region of large displacement shifts, which generated the intensive tsunami waves. As stated previously the main displacements in the source region occurred during the first 150 sec after the main shock (Fujii 2011).

The grey dotted lines outline the region of the first-day aftershocks of the earthquake. Also shown in fig.1 is the region of historical earthquakes, which occurred in 1896 and 1933. The blue dashed curve shows regions of the strongest earthquakes, and the violet-colored points correspond to the assumed region of the strongest tsunami in the region, which occurred in the year 869 (Fujii 2011).

2. STATEMENT OF THE PROBLEM

Following the 2011 Tohoku-Oki earthquake, researchers from many countries performed numerical simulations of the tsunami event, using different approaches in generally stating the problem and in the numerical simulation itself (Kanamori 2011, Yomogida 2011, Baranova et.al. 2014, Hayashi 2011, Lovholt 2012, Imamura 2011,).

The structuring and initial configuration of the tsunami source area depends primarily on the character and the dynamics of crustal and sedimentary displacements within the earthquake source region. Presently, a number of mathematical models exist which numerically simulate a tsunami by taking into consideration the real geometry and the initial tectonic displacements of the seafloor (see, e.g. Kurkin 2004, Lobkovsky L.I., 2006). However, the determination of initial sea bottom displacements that contribute to tsunami generation is somewhat indefinite and depends on different possible scenarios. One of the present widely-used methods (see Okada 1985, Okada 1992, Imamura 2011) relates to the choice of orientation of longitudinal and transverse faults at the seismic source regions and on estimates of displacements along the rupture zone, which are difficult to evaluate and determine because of the extensive variability of such displacements for different events along and within different subduction zones. (Okada 1985, Okada 1992).

Based on earthquake magnitude alone, there are various correlation expressions being used to estimate the specific tsunami source characteristics. However, in order to determine the source parameters of tsunami generation, in addition to earthquake magnitude, it is essential to establish the vertical components of displacements of the sea floor and the orientation of the quake's rupture plane in the source region (Wells 1994). The displacement distribution on the sea floor for the case of a rectangular area of rupture is usually calculated with certain described formulas (Okada 1992). Furthermore, such studies use a solution of the static displacement of source segments in elastic semi-space, as calculated from crustal displacement distribution on its surface, which are then used to simulate a tsunami (Okada 1985, Okada 1992).

Another method in obtaining horizontal and vertical shifts within the tsunami source region has been presented in the literature (Lobkovsky 1988, Lobkovsky and Baranov 1984, Garagach and Lobkovsky 2006). It is well established that the strongest earthquakes near volcanic island arcs occur near the plane of contact between the base of the subducting plane and of the island arc

wedge and the most significant crustal displacements result of rupturing initiated along the plane of contact. As these studies demonstrate, the island arc wedge comprises separate large segments, which have been formed by transverse faulting. The presence of the faulting permits the introduction of new, smaller scale elements of interaction – keyboard blocks on the frontal edge of overriding plate (Lobkovsky 1988, Lobkovsky and Baranov 1984). Recent studies (Garagach and Lobkovsky 2006, Garagach and Ermakov 2001), are based on an elaborate geo-mechanical model in the subduction zone, based on the premise that the initial stress distribution affects essentially the crustal motion character near the earthquake source. Thus, taking into account the stress-strained state of keyboard blocks to obtain the dynamical components of vertical shift within the earthquake source area, a numerical simulation was performed on the processes within the seismic source (scenario 2), based on the program with the code name FLAC (dynamical keyboard model) (Lobkovsky 1988, Lobkovsky and Baranov 1984, Garagach and Lobkovsky 2006, Garagach and Ermakov 2001, Lobkovsky et al. 2006).

Using the two models in the present study, we performed a comparative numerical simulation of the tsunami generation source parameters and of the successive propagation of the tsunami in the Pacific Ocean basin.

3. SOURCE FORMATION OF THE TOHOKU 2011 TSUNAMI

3.1. Scenario 1

For a tsunami source for the first scenario, we used the seismic source described in the literature (Okada 1985, Okada 1992, Imamura 2011). This source was constructed on parameters of the ten strongest aftershocks, which occurred for some time interval (fig. 2).

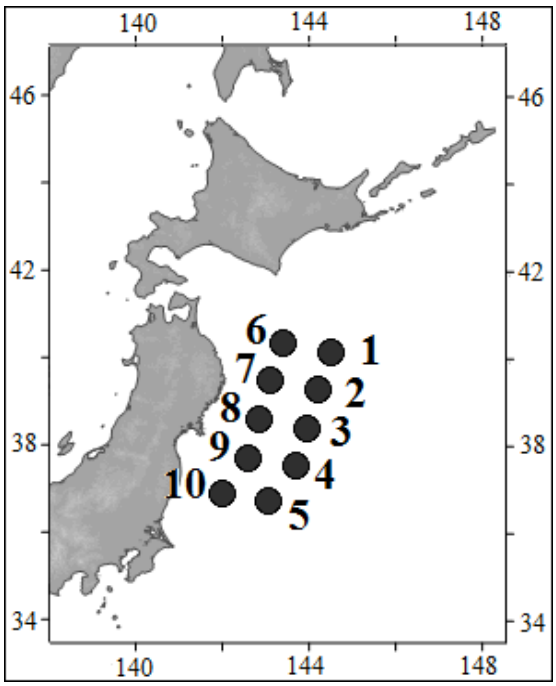

Figure 2. Aftershock locations of the earthquake of 11 March 2011 (Imamura 2011)

The distribution of vertical displacements on the sea bottom for a given source was calculated with formulas described by Okada (Okada, 1992). This source comprises of ten segments moving in different time intervals. The parameters that were used are the same for all the segments. Specifically, the length and width of the fault are the same (100 km). The fault rupture orientation (the strike angle) is 193°. The angle of plate inclination (the dip angle) is 14°, and the angle of plate displacement (slip angle) is 81°.

Based on the earthquake source parameters given in Table 1, one can obtain the heights of water level displacement at the source for each segment, using Okada's solution (Okada 1985, Okada 1992). Shown in columns 2-5 of Table 1, are the seismological and geodynamic data (Okada 1992, Imamura 2011), which was recalculated with the Okada formula. The last column shows the calculated initial displacement of water level at the tsunami source, as obtained with the same formula (Okada 1985, Okada 1992).

Table 1. The basic parameters of a seismic source (Kostenko et al. 2013).

Number of segment	Epicenter coordinates	Depth of source, km	Vertical displacement of source, m	Segment activation time, sec	Maximum displacement of water level, m
	1	2	3	4	5
1	40,168 N., 144,507 E.	1	20	0	12.49
2	39,300 N, 144,200 E.	1	10	0	6.24
3	38,424 N., 143,939 E.	1	35	30	21.87
4	37,547 N., 143,682 E.	1	15	30	9.37
5	36,730 N., 143,070 E.	1	2,5	60	1.56
6	40,367 N., 143,394 E.	24	1	60	0.5
7	39,496 N., 143,100 E.	24.2	3	90	1.5
8	38,620 N., 142,853 E.	24.2	4	90	1.99
9	37,744 N., 142,609 E.	24.2	2	120	0.99
10	36,926 N., 142,009 E.	24.2	2	120	0.99

The formation of the surface water wave for each segment (see Table 1) is presented in fig. 1. Immediately after the onset of the main event, segments 1 and 2 contribute to the initial sea level disturbance. After a time interval of about 30 sec, other source segments contribute to tsunami generation. The generation process is completed by the sea level displacements in segments 9 and 10. The process in whole occurs during a time interval of 120 seconds. As seen, all ten segments contribute to a bipolar type of displacement of wave level, which has a complex

form. The depression of sea level (blue color) faces the coasts of Honshu and Hokkaido islands, while the elevated sea level (yellow-red color), faces towards the open ocean.

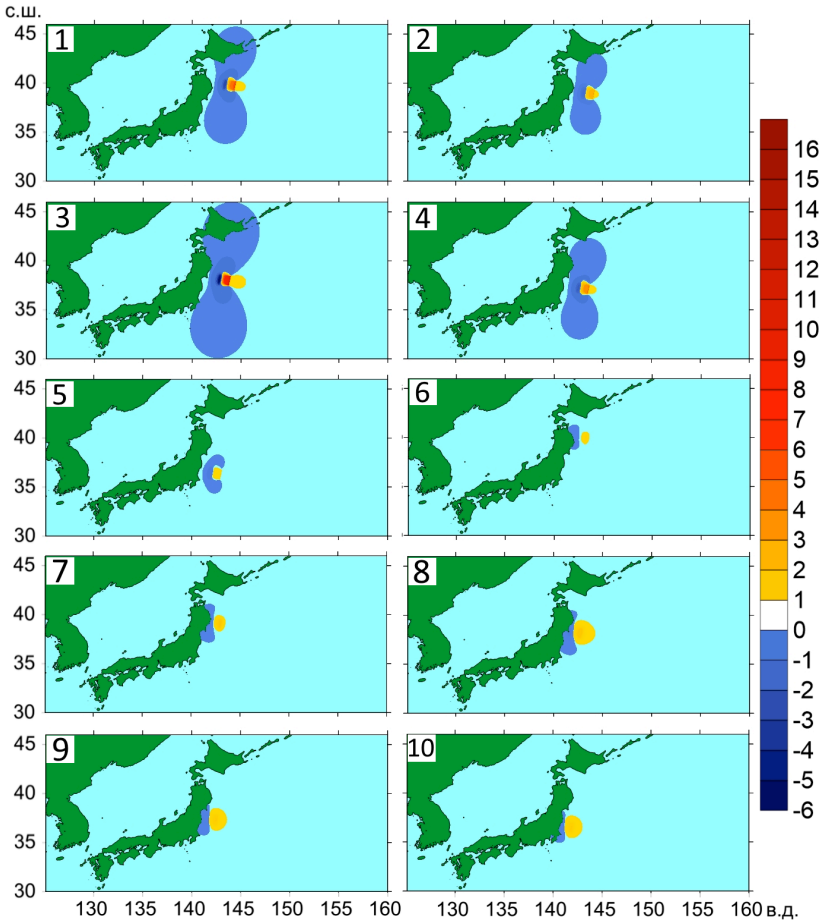

Figure 3. Formation of a tsunami source for scenario 1.

3.2. Scenario 2

The form of the seismic source for Scenario 2 was determined using data from NOAA's Center for Tsunami Research (http://nctr.pmel.noaa.gov/ honshu20110311/ namidance.ce.metu.edu.tr/; and from other researched (Lobkovsky and Baranov 1984, Baranova et al. 2014) (fig.4). For our numerical simulation processes of tsunami generation, the seismic source was that of Baranova et al. (2014) (see fig.4a).

To construct a geomechanical model of the subduction zone, a velocity cross-section was used as that described in recent work (Garagach and Ermakov 2001, Garagach and Lobkovsky 2006). Such a model takes into account both the density distribution and the distribution of tectonic stresses in the Earth's crust (Garagach and Ermakov 2001, Garagach and Lobkovsky 2006). Using data from other research work (22; Takahashi 2004), a numerical simulation of processes in seismic source was performed based on the program code FLAC (Baranova et al., 2014**,** Garagach and Lobkovsky, 2006)**.**

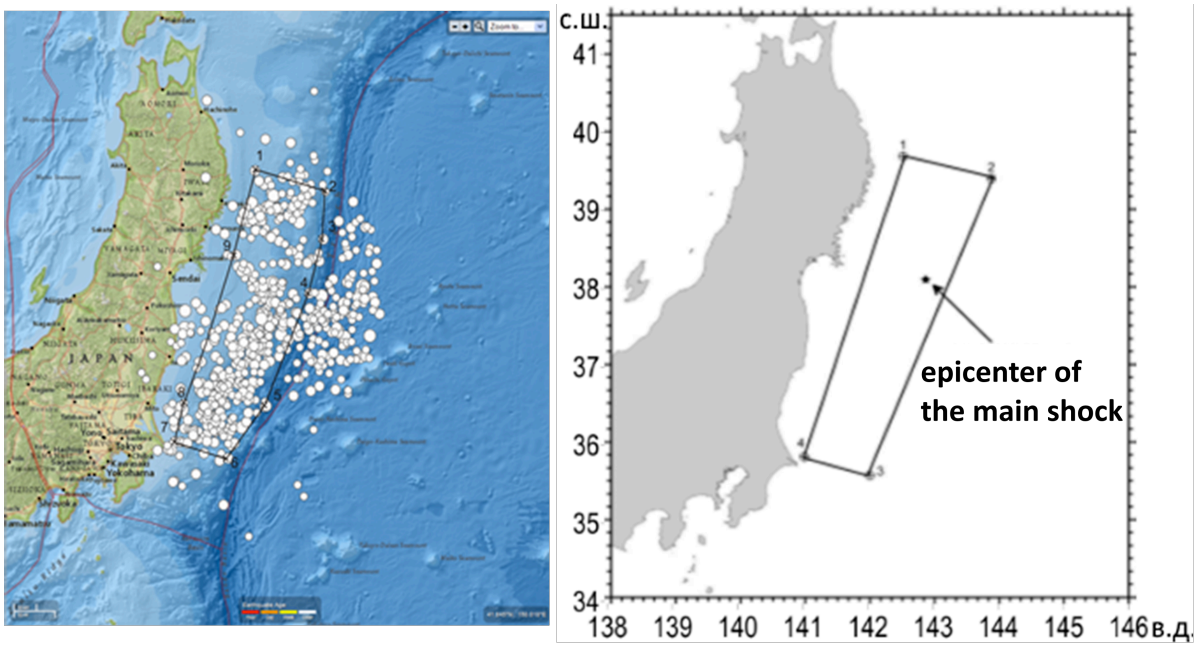

Fig. 4. a) Source of Tohoku earthquake of aftershocks of the first day. b) Simplified shape of earthquake source used under computation (Baranova et al. 2014).

The computational scheme in depicting the earthquake source zone is illustrated in Fig. 5. Apparently, and as also illustrated in Fig. 6, there was an accumulation of crust deformation intensity within the seismic source, which contributed to the distribution of vertical displacement during the pre-earthquake period (Baranova et al. 2014).

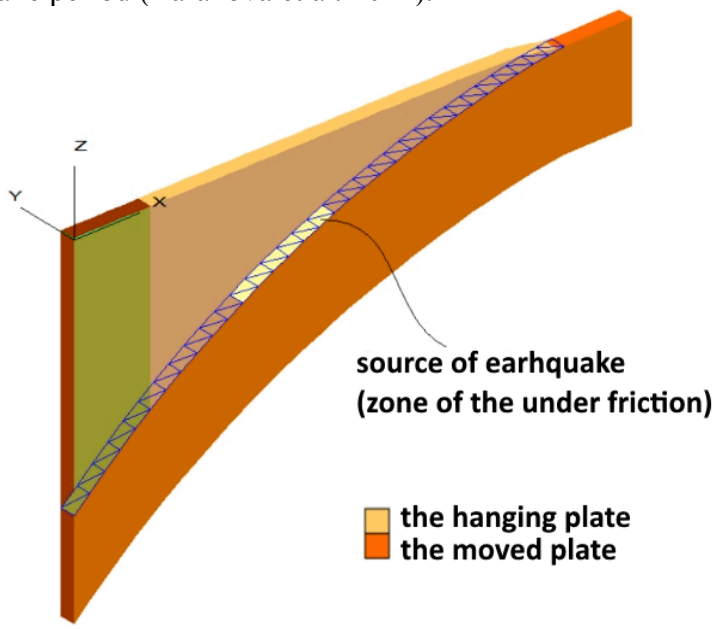

Figure 5. Calculated scheme of a zone of an earthquake source (Baranova et al. 2014, Garagach and Lobkovsky 2006).

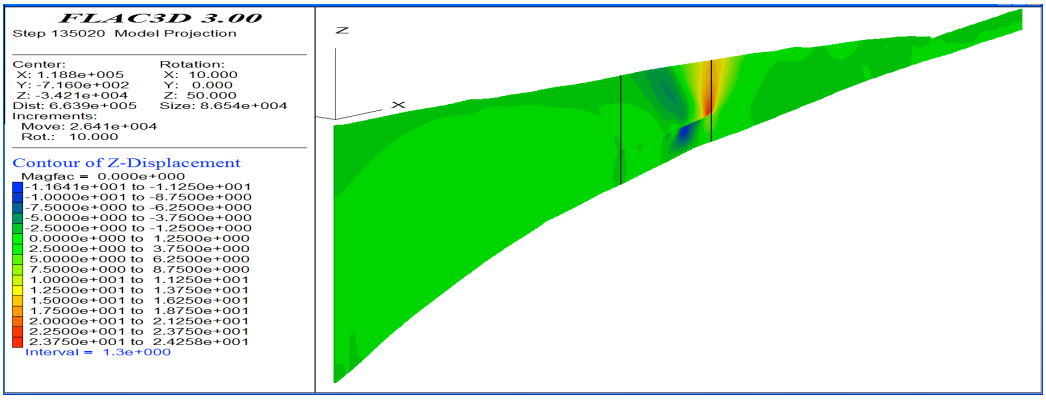

Figure 6. Vertical displacement after an earthquake. Vertical lines selected a section on which there was a reduction of friction coefficient (Baranova et al. 2014, Garagach and Lobkovsky 2006).

In our study, we examined the earthquake source as a motion of a single block which extended from 70 to 150 km (Fig. 5,6) on the X-axis - as delineated graphically in Fig. 7 - taking into account the intensity of the initial stress before the occurrence of the main earthquake (Garagach and Ermakov 2001, Garagach and Lobkovsky 2006), which Baranova et al. (2014), calculated within the frames of the program coded as FLAC. Illustrated by Fig. 7 are the changes of vertical displacement of the sea floor during the earthquake in the seismic source region from its beginning $t = 0$ for a time period $t = 135$ seconds.

The beginning of the earthquake process was very indistinct, particularly during the first five seconds. During the time interval of 30-45 seconds, the crustal expansion accelerated and the displacements amplified. After this time period, the rupture continued for another 45 seconds in a northern direction and terminated 135 seconds after the onset of the main earthquake. (Fujii 2011, Koper et al. 2011, Kanamori 2011).

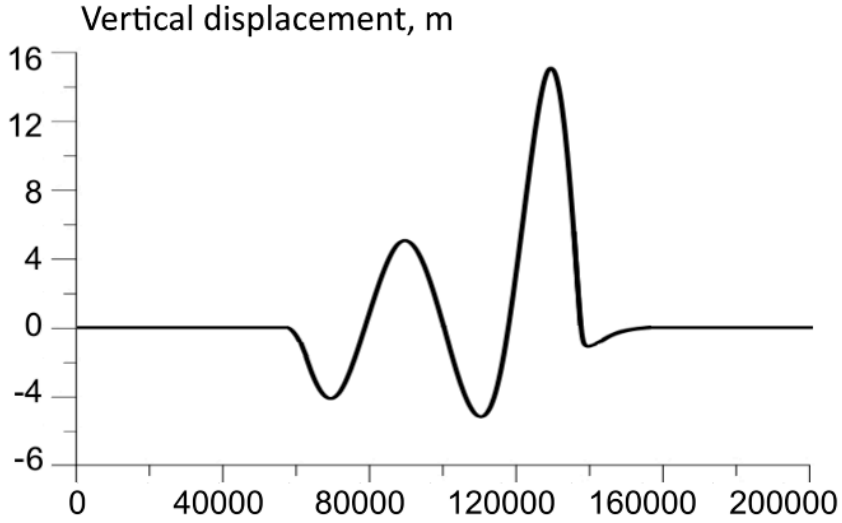

Figure 7. Plots of change of vertical displacements (Baranova et al., 2014).

4. NUMERICAL MODELING

The analysis of the two scenarios was performed by numerical simulation using square block areas which extended from 120˚ E - 115˚ W, from 60˚ N – 60˚ S, from 120˚ E - 160˚ E, and from 30˚ N – 46˚, along the eastern Pacific coast of Honshu Island. One of the computation basins is presented in Fig. 8. The bathymetry of this region was taken from the GEBCO Digital Atlas, which has a 30-arcsec resolution [5]. The grid step for the analysis averaged about 900 meters.

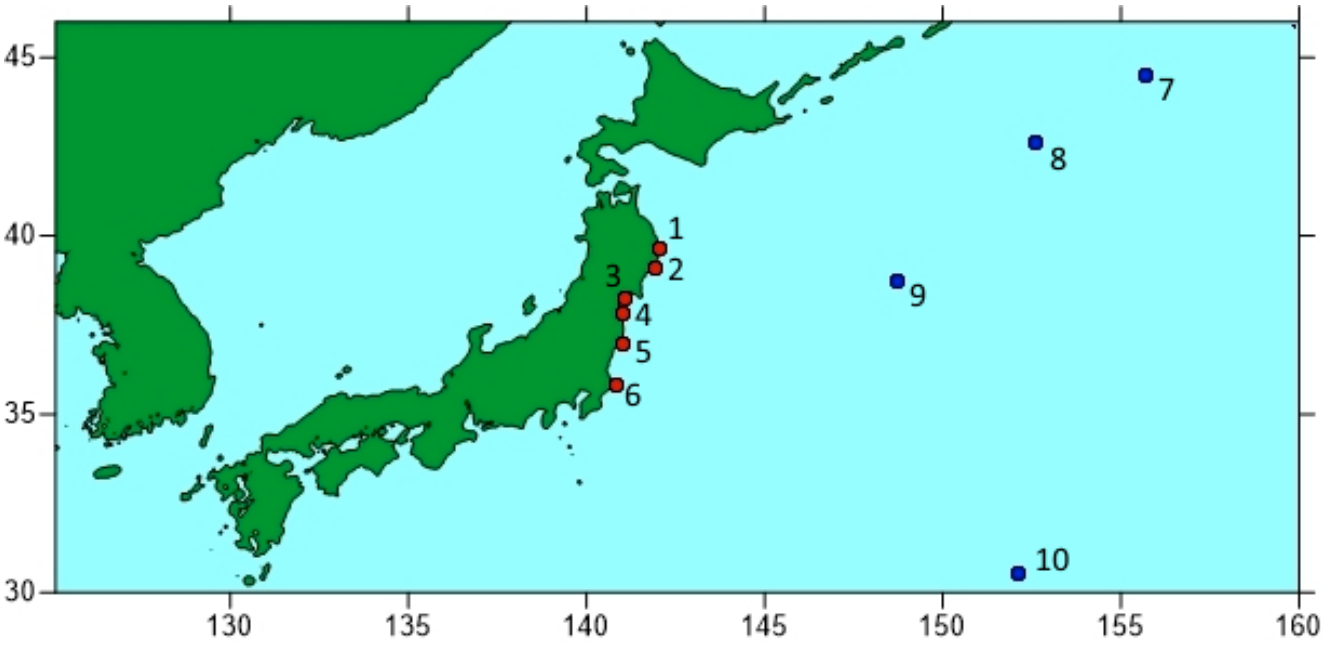

Figure 8. The computational area. The red points 1-6 correspond to the assigned position of virtual tide gauges along the coastal zone; the blue points 7-10 correspond to position of the measuring DART instruments.

To compare the results of the numerical simulation and for comparison with the observational data, virtual tide-gauges were chosen along coastal location points of Honshu Island in Japan where the maximum measurements of sea levels had been observed (Fig. 9). However, some differences in the location of computational points and of the real tide gauges, connected with technical features of numerical simulation, can lead to some dispersion in the record of the height and period of sea level oscillations.

4.1. Scenario 1

The numerical simulation of Scenario 1 was realized by using the program complex NAMI DANCE [31], which solves the shallow water equations written in spherical coordinates and by taking into account the Earth's rotation (Coriolis Force):

$$\frac{\partial M}{\partial t}+\frac{1}{R\cos\theta}\frac{\partial}{\partial\lambda}\left(\frac{M^2}{D}\right)+\frac{1}{R\cos\theta}\frac{\partial}{d\theta}\left(\frac{MN\cos\theta}{D}\right)+\frac{gD}{R\cos\theta}\frac{\partial\eta}{\partial\lambda}+\frac{gn^2}{D^{7/3}}M\sqrt{M^2+N^2}=fN,$$
$$\frac{\partial N}{\partial t}+\frac{1}{R\cos\theta}\frac{\partial}{\partial\lambda}\left(\frac{MN}{D}\right)+\frac{1}{R\cos\theta}\frac{\partial}{d\theta}\left(\frac{N^2\cos\theta}{D}\right)+\frac{gD}{R}\frac{\partial\eta}{\partial\theta}+\frac{gn^2}{D^{7/3}}N\sqrt{M^2+N^2}=-fN, \quad (3)$$
$$\frac{\partial\eta}{\partial t}+\frac{1}{R\cos\theta}\left[\frac{\partial M}{\partial\lambda}+\frac{\partial}{\partial\theta}(N\cos\theta)\right]=0$$

where η is a sea level change, M and N are components of water discharge along latitude λ and longitude θ; D is the total depth of the basin; g is the gravity acceleration; R is the Earth's radius, f is the Coriolis parameter and n is the bottom friction coefficient. For the computation, the value n = 0.0015 $m^{-1/3}c$, is used which is characteristic for natural bottom (sand, pebbles). The equations are solved within the framework of the nonlinear dispersion theory of long waves, where physical dispersion is replaced by a numerical one (Kostenko et.al. 2013). Under the present simulation a time step in 1 sec was used, thus satisfying the Courant condition. At the open Pacific front, the boundary conditions are stated in the form of free wave passing.

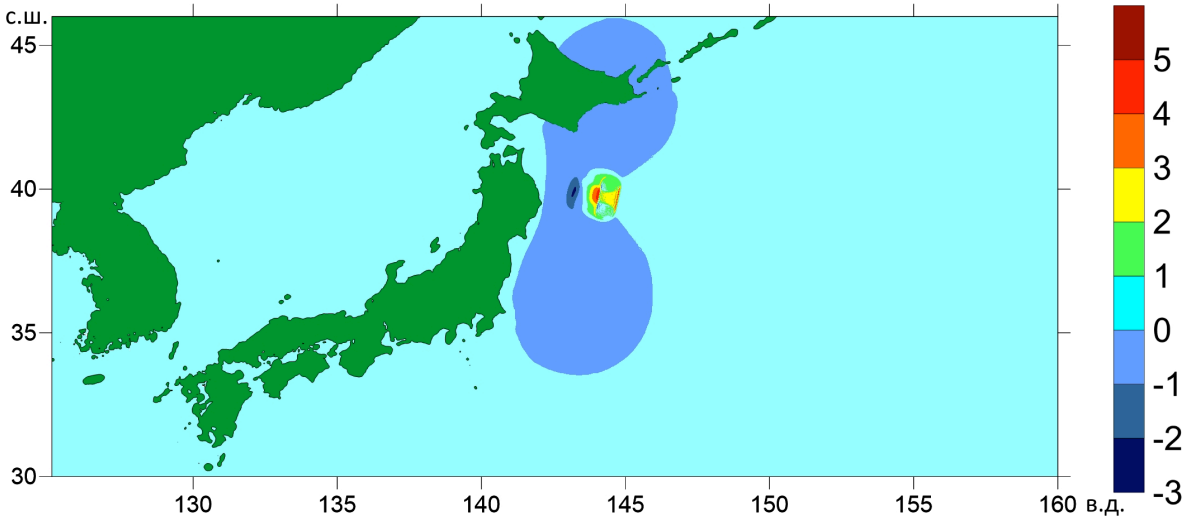

Figure 9. The tsunami source generated on 120 sec (Scenario 1).

Presented in fig. 9 is the areal configuration of the tsunami source, taking into consideration all of the 10 segments of block displacements – after an interval of 120 seconds from the onset of the main quake. Presented In fig.10 are the advancing tsunami wave fronts for six time moment intervals. As shown, practically at all coastal points of Honshu and Hokkaido islands, the tsunami is initiated with a withdrawal of seawater from the beaches. A clearer illustration of the distribution of maximum tsunami wave height on the basin is presented in fig. 11.

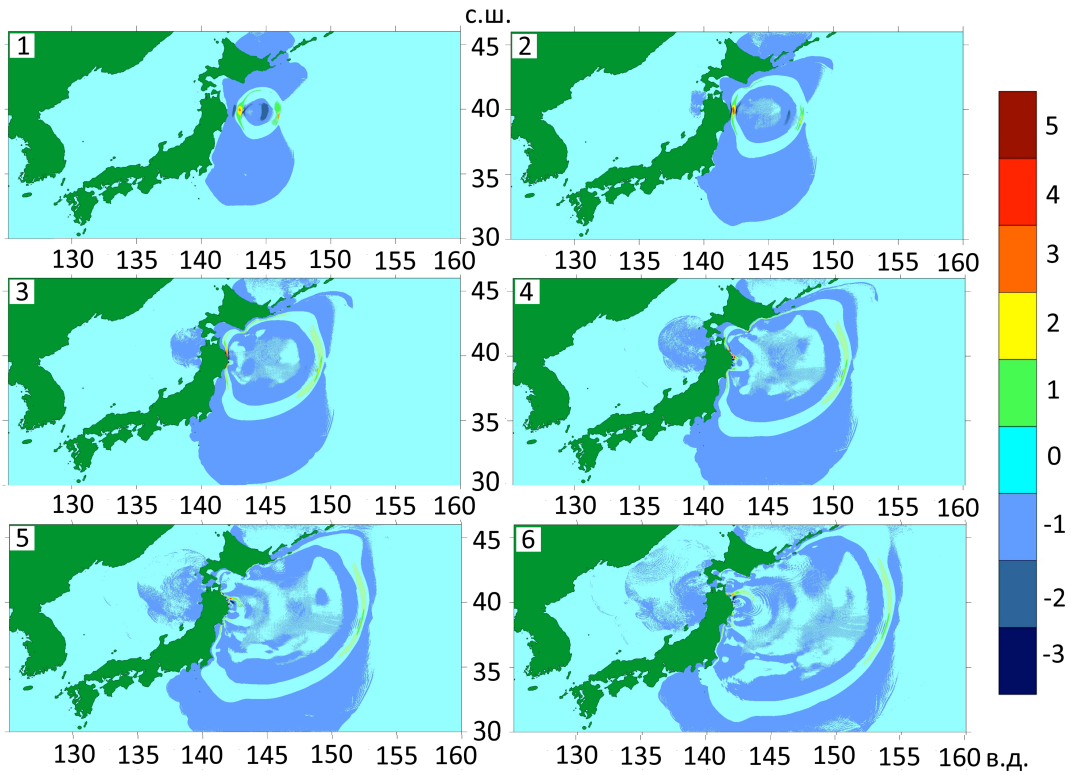

Figure 10. Position of wave fronts for 6 time moments ranging: 1 - 10 min, 2 - 20 min, 3 - 30 min, 4 - 40 min, 5 - 50 min, 6 - 60 min.

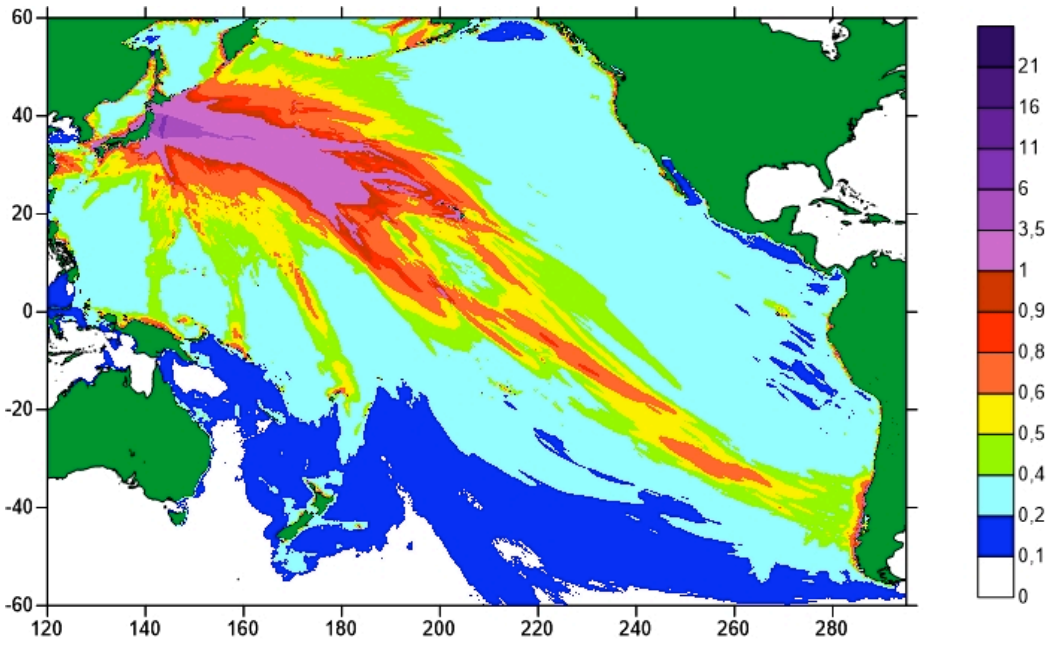

Figure 11. Maximum distribution of tsunami wave energy flux in the Pacific Ocean based on implementation of scenario 1.

4.2. Scenario 2

The tsunami source for Scenario 2 was determined by use of the dynamical keyboard model (Lobkovsky 1988, Garagach and Ermakov 2001, Garagach and Lobkovsky 2006, Lobkovsky, Mazova et al. 2006).

To describe the tsunami simulation from the earthquake source, a system of nonlinear shallow water equations was used as described in the scientific literature (Lobkovsky, Mazova et al. 2006). A system of nonlinear shallow-water equations (as in Lobkovsky at el. 2006) was used for the numerical simulation of tsunami generation from the 2011 Tohoku, Japan earthquake as follows:

$$\begin{cases} \dfrac{\partial u}{\partial t} + u\dfrac{\partial u}{\partial x} + v\dfrac{\partial u}{\partial y} + g\dfrac{\partial \eta}{\partial x} = f_1 \\ \dfrac{\partial v}{\partial t} + u\dfrac{\partial v}{\partial x} + v\dfrac{\partial v}{\partial y} + g\dfrac{\partial \eta}{\partial y} = f_2 \\ \dfrac{\partial \eta}{\partial t} + \dfrac{\partial}{\partial x}[(\eta + H - B)u] + \dfrac{\partial}{\partial y}[(\eta + H - B)v] = \dfrac{\partial B}{\partial t} \end{cases} \tag{6.1}$$

where $f_1 = \dfrac{-C_h}{H+\eta} u\sqrt{u^2+v^2}$, $f_2 = \dfrac{-C_h}{H+\eta} v\sqrt{u^2+v^2}$ are the bottom friction; *x,y* are the space coordinates along the axes *Ox* and *Oy,* respectively; *t* is the time; *u*(*x*, *y, t*), *v(x, y, t)* are the average over depth horizontal components of fluid flow rate; $\eta(x,y,t)$ is the displacement of free surface relatively its undisturbed level; *H* is the maximum depth of the basin at undisturbed water, function $B(x,y,t)$ describes displacement of bottom surface relatively initial position (accounting to dynamic characteristics of seismic motion); g is the gravity acceleration, $Ch = \dfrac{(H+\eta-B)^{0.4}}{sh}$ is the bottom friction coefficient (Shezi coefficient), and sh is the roughness coefficient.

Figure 12 depicts four time moments of the tsunami source generation of the Tohoku 2011 earthquake for Scenario 2 (see fig. 7). The two peaks of vertical change in this figure are shown in yellow and red colors (2 and 4 panels). To two minimums in the same figure 12 are shown in dark-blue and blue colors (1 and 3 panels). After the formation of the tsunami source, the wave begins to propagate towards both the coast of Honshu Island and the open ocean.

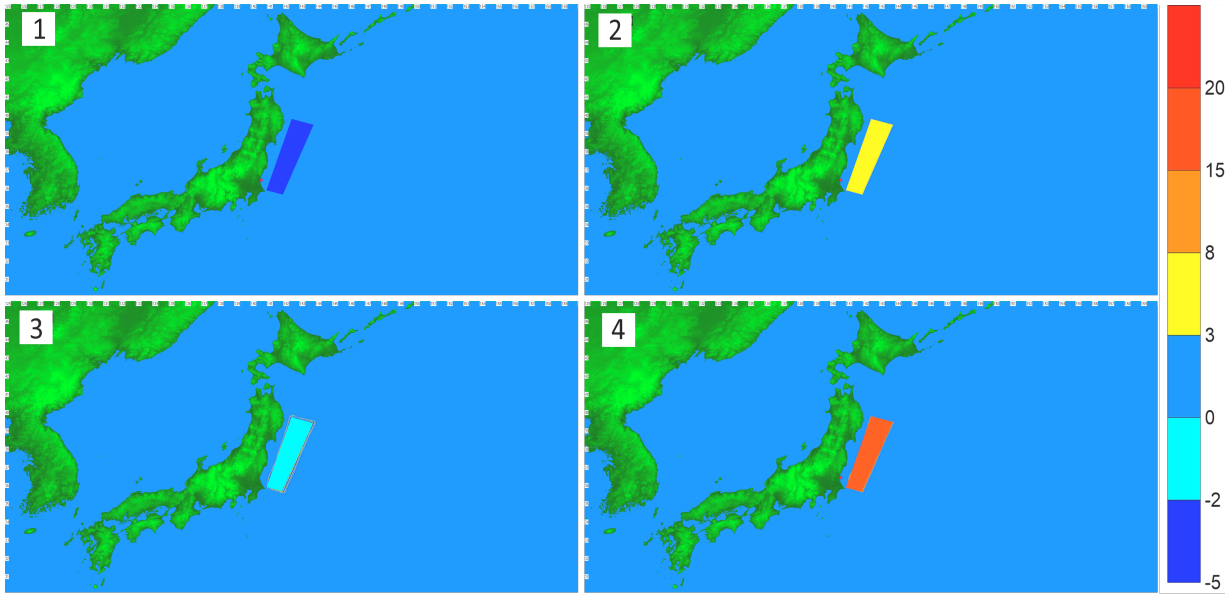

Fig.12. Generation of the dynamic source (scenario 2). 1. H= -4 m. 2. H = +5 m. 3. H = -5 m. 4. H = +15 m.

Fig.13 shows the propagation of the wave fronts for six time moments. It is well seen from the simulation that the initial tsunami wave at Honshu Island arrives in 15-20 min, and that the maximum tsunami wave height at Miyako is more than 20 meters. At Hokkaido island the tsunami wave arrives in 32 minutes and that a wave with a maximum height near 3.6m arrives at Erimo in 58 minutes.

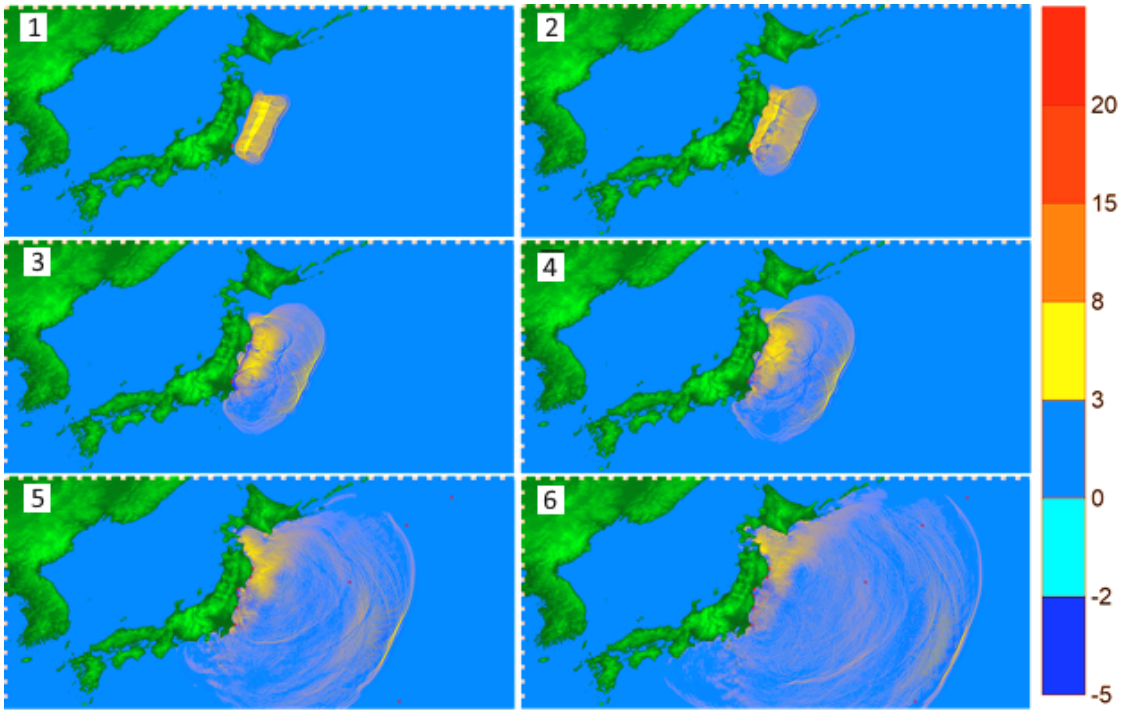

Fig.13. Position of wave fronts for time moments: 1 – 10 min,2 - 20 min, 3 – 25 min, 4 – 30 min, 5 – 45 min, 6 – 60 min. 2- 20 мin, 3 – 25 мin, 4 – 30 мin, 5 – 45 мin, 6 – 60 мin.

Fig.13 shows the distribution of computed maximum tsunami wave heights based on the implementation of scenario 2. As shown, the greater intensity of wave energy focuses on the central part of Honshu Island. Near Hokkaido Island and the Kurile islands, the wave heights are not larger than 7-8 meters.

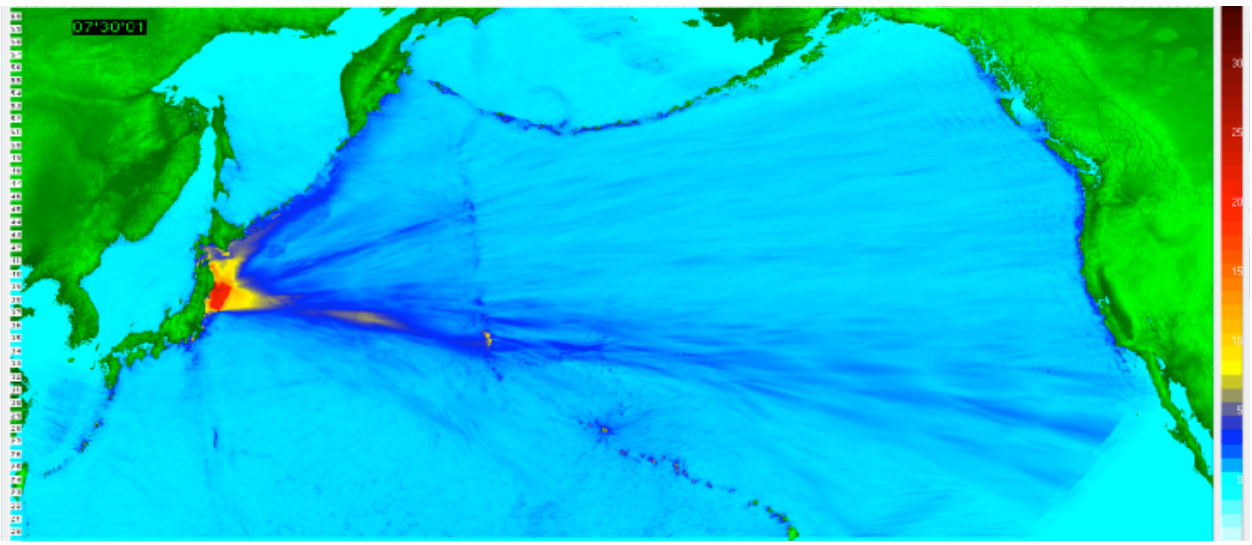

Fig.14. Maximum distribution of waves in the water area of the Pacific Ocean in case of implementation of the scenario 2.

4.3 Comparison of real data and results of calculations with the Okada model (Okado 1992) and the model of dynamic source (Baranova et al. 2014).

The results of computation for the first and second tsunami waves for the 2011 Tohoku Japan event that were performed with the Okada model as well as with the dynamic source are presented in Table 2. Shown in the first line of the column with the heading «Coordinate pp», are the coordinates of the of real event (from Saito et al. 2011) and in the second line the coordinates of the virtual tide gauges.

As seen from Table 2, for a number of coastal points as for example Miyako, for both first and second scenarios there is good agreement between the observed/recorded data from tide gauges and the results of the numerical simulation. Antithetically, from Sendai to Choshi the agreement between computed and observational data is noticeably poorer. At Ofunato, the computation with the model of dynamical source gives somewhat good agreement with the observational data, particularly for the second wave. However, at Goshi, although the tide gauge data shows the first wave to be a positive flooding wave followed by a negative wave of withdrawal, the computation data in both models gives a reciprocal picture, and at all computation points the tsunami begins with the withdrawal of water from a beach which is accompanied by second depression wave. Since such a picture is observed for both Scenario 1 and Scenario 2, which are independent from one other, such differences of the data can be associated with small-scale bottom relief features at this part of the shelf. At the deep-water DART tsunami recorders, the picture is essentially better

and the computed phase relations of the wave are consistent with the observational data. The first wave is a positive elevation wave, followed by a depression wave. For DART21-401 station the computed and observation data are in agreement for both models. For DART21-419 station, the results of computations with the dynamic model are in better agreement with the observational data while for station DART21-418 the agreement of computed and observation data is better with the Okada model. In the case of station DART21-413, the observation data is in good agreement only with computation of the second wave (depression wave) using the Okada model.

Table 2

N	Points	Coordinate pp. 1.Real data 2.Scenario 1 3.Scenario 2	Real data		Scenario 1		Scenario 2	
			1		2		3	
			First wave	Second wave	First wave	Second wave	First wave	Second wave
1	Miyako	141.9830 39.6500 142.0662 39.6433	-1.2	+7.7	-2.7	+6.8	-1.1	+7.8
2	Ofunato	141.7500 39.0170 141.9161 39.0594	-2	+7	-1.3	+2.7	-1.2	+7
3	Sendai	141.0330 38.2670 141.0653 38.2252	-1.3	+5	-0.3	+1.6	-0.8	+3.3
4	Soma	140.9500 37.8170 141.0486 37.7914	-1.8	+8.7	-0.19	+1.7	-1.4	+5.7
5	Onahama	140.8833 36.9369 140.9985 36.9405	-0.7	+2	-0.1	+0.6	-1.1	+4.2
6	Choshi	140.8670 35.7500 140.8651 35.7893	+2	-1	-0.1	+0.7	-0.7	+2.5
7	DART21 419	155.7000 44.5000 155.6959 44.5151	+0.7	-0.2	+0.35	-0.63	+0.75	-0.3
8	DART21 401	152.6000 42.6000 152.6096 42.6131	+0.8	-0.2	+0.9	-0.6	+0.5	-0.3
9	DART21 418	148.7000 38.7000 148.7059 38.7090	+2	-1	+1.87	-0.88	+1,.2	-0.5
10	DART21 413	152.1000 30.5000 152.1091 30.5005	+0.7	-0.2	+0.3	-0.24	+0.4	-0.3

5. CONCLUSIONS

Since in the near-field zone the tsunami generation mechanisms are affected by both the configuration and the dynamics of the seismic source, there is an obvious difference between the values of tsunami wave height obtained with both Scenarios 1 and 2 of the present study. On the other hand, at a distance of more than three tsunami wavelengths, both the shape and the influence of the seismic source area become less essential. This is probably the reason that more consistent values are obtained for deep-water DART tsunami stations for both Scenarios 1 and 2. As for the comparison with values of wave heights from real tide gauges, an essential factor of differences are their location as compared with the chosen locations of virtual tide gauge stations - since in the coastal zone there are essential effects of amplification due to convergence of the waves, in

addition to subsequent reflections. So, for rough estimates of numerical simulation of tsunami generation and propagation of waves using both for Models 1 and 2, it can be concluded that for near-field sources (for coasts of Honshu and Hokkaido islands) most coastal points do not demonstrate a good agreement with the data obtained from tide gauges and that can be attributed to both coastal configuration and features of the local submarine relief. However, for far-field regions the values of maximal wave height are in better agreement. Finally, it should be emphasized that an important factor is also the initial crustal stress distribution before the earthquake's onset.

ACKNOWLEDGEMENTS

The presented results were obtained within the framework of the state order in the sphere of scientific activity (Tasks № 2015/133 ("organization of scientific research" and project No. 2839).

REFERENCES

1. Baranova N., Baranov B., Lobkovsky L., Mazova R., 2014. New approach to the analysis of strongest earthquake Tohoku 2011: Int. Workshop on Mega Earthquakes and Tsunamis in Subduction Zones: Forecasting Approaches and Implications for Hazard Assesment (Rhodes Isl., Greece, 6-8 October, 2014), Abstr. Book, p.23-24.
2. Fujii Y., 2011. Tsunami source of the 2011 off the Pacific coast of Tohoku Earthquake: Earth Planets Space Letters, 63, pp.815–820.
3. Garagash I.A., Lobkovsky L.I., 2006. An analysis of the dynamic displacement process of the sea bottom due to a subduction zone earthquake: 4th International FLAC Symposium on Numerical Modeling in Geomechanics – 2006. Symp.Proc. (Hart & Varona (eds.)) pp.06-01.
4. Garagash I.A., Ermakov V.A., 2001. Using of geology-geophysical models for modeling of stressed state of Earth crust on example of Sakhalin island and North Tyan-Shan: III Scientific Conference "Problems of seismicity of Far East", Khabarovsk, Russia, 2001. Conf. Proc. pp.23-27.
5. GEBCO world map. URL: http://www.gebco.net/data_and_products/gebco_world_map/
6. Hayashi Y. et al., 2011. Tsunami source area of the 2011 off the Pacific coast of Tohoku Earthquake determined from tsunami arrival times at offshore observation stations: Earth Planets Space Letters, 63, pp.809–813.
7. Hirose F., Miyaoka K., Hayashimoto N., Yamazaki T., Nakamura M., 2011. Outline of the 2011 off the Pacific coast of Tohoku Earthquake (M_w 9.0): Seismicity: foreshocks, mainshock, aftershocks, and induced activity: Earth Planets Space. 63. pp. 513–518.
8. Ito Y., Tsuji T., Osada Y.,. Kido M, Inazu D., Hayashi Y. et al., 2011. Frontal wedge deformation near the source region of the 2011 Tohoku-Oki earthquake: Geophys. Res. Lett. 38, p. L00G05, DOI:10.1029/2011GL048355.
9. Imamura F., 2011. Tohoku University Source Model version 1.0 of Great East Japan Tsunami. (Due on June 06, 2011).

10. JAMSTEC.URL:http://www.jamstec.go.jp/j/about/pressrelease/20110428/
11. Japan Meteorological Agency. URL: http://www.jma.go.jp/jma/ indexe.html
12. Koper K.D., Hutko A.R., Lay T., Ammon C.J., Kanamori H., 2011. Frequency-dependent rupture process of the 2011 M_w 9.0 Tohoku Earthquake: Comparison of short-period P wave back projection images and broadband seismic rupture models: Earth Planets Space. 63. pp. 599–602.
13. Kanamori H., Yomogida K. (Guest Eds.), 2011. First Results of the 2011 off the Pacific coast of Tohoky Earthquake / In: Earth Planets Space, Special Issue. 63.
14. Kurkin A.A., Pelinovsky E.N., Choi B.H., Li D.S., 2004. A comparative estimation of the tsunami hazard for the Russian coast of the Sea of Japan based on numerical simulation: Oceanology 44, pp.163-172.
15. 15.Kostenko I.S., Zaitsev A.I., Yalchenir A., Rybin A.V., Yarkin D.C., 2013. Manifestation of 2011'th Tohoku tsunami near Kuril islands and Sakhalin island: Transactions of NNSTU n.a. R.E. Alekseev. 2 (99), pp. 43-51.
16. Lay T., Kanamori H., 2011. Insights from the great 2011 Japan earthquake: Phys.Today 64, pp.33-39.
17. Lovholt F. et al., 2012. Modeling propagation and inundation of the 11 March 2011 Tohoku tsunami: Nat. Haz. Earth Syst. Sci., 12, pp.1017–28.
18. Lobkovsky L.I., 1988. Geodynamics of spreading and subduction zones and two-level plate tectonics(Nauka Press, Moscow, USSR, 1988).
19. Lobkovsky L.I., Baranov B.V., 1984. Keyboard model of strong earthquakes in island arc and active continental edges: Doklady, 275, pp.843-847.
20. Lobkovsky L.I., Mazova R.Kh., Kataeva L.Yu., Baranov B.V., 2006. Generation and propagation of catastrophic tsunami in basin of Okhotsk Sea. Possible scenarios: Doklady, 410, pp.528-531.
21. Magnitude 8.9 – NEAR THE EAST COAST OF HONSHU, JAPAN 2011 March 11 05:46:23 UTC. URL: http://earthquake.usgs.gov/earthquakes/recenteqsww/Quakes/busc0001xgp.php .
22. NOAA Center for Tsunami Research – http://nctr.pmel.noaa.gov/ honshu20110311/ namidance.ce.metu.edu.tr/
23. Mori, N., and Takahashi T. 2012. The 2011 Tohoku Earthquake Tsunami Joint Survey Group, 2012. The 2011 Tohoku Earthquake Tsunami Joint Survey Group (2012), Nationwide Post Event Survey and Analysis of the 2011 Tohoku Earthquake Tsunami, Coastal Engineering Journal, Vol. 54, Issue 4, 1250001, 27 p, doi:10.1142/S0578563412500015
24. Okada Y., 1985. Surface deformation due to shear tensile faults in a half-space: Bull. of the Seismological Society of America, 75, pp.1135-1154.
25. Okada Y., 1992. Internal deformation due to shear and tensile faults in a half-space: Bull. Seismol. Soc. Am., 82, pp.1018–1040.
26. Pararas-Carayannis G., 2014. The Great Tohoku-Oki Earthquake and Tsunami of March 11, 2011, in Japan. Pure Appl. Geophys. 171, 3257-3278, Springer, DOI 10.1007/s00024-013-0677-7 Erratum on the distribution of inundation and wave heights along the coastline of Eastern Honshu as determined by the comprehensive survey summarized by Mori et al. (2011) and by Mori et al. (*2012*) or other investigations.

27. Saito T., Ito Y., Inazu D., and Hino R., 2011. Tsunami source of the 2011 Tohoku-Oki earthquake, Japan: inversion analysis based on dispersive tsunami simulations: Geophys. Res. Lett. 38.
28. Takahashi N. et al., 2004. Seismic structure and seismogenesis off Sanriku region, northeastern Japan: Geophys. J. Int. 159, pp.129-145.
29. Wells D.L., Coppersmith K.J., 1994. New empirical relationships among magnitude, rupture length, rupture width, rupture area, and surface displacement: Bull. Seism. Soc. Am. 84, pp. 974-1002.
30. Yomogida K, Yoshizawa K, Koyama J, and Tsuzuki M., 2011. Along-dip segmentation of the 2011 off the Pacific coast of Tohoku Earthquake and comparison with other megathrust earthquakes: Earth Planets Space, 63, pp.697–701.
31. NAMIDANCE URL: http://avi-nami.ce.metu.edu.tr , http://namidance.ce.metu.edu.tr/